

Zeolite Synthesis

Solvent-Free Syntheses of Hierarchically Porous
Aluminophosphate-Based Zeolites with AEL and AFI StructuresYinying Jin,^[a, b] Xian Chen,^[a] Qi Sun,^[a] Na Sheng,^[a] Yan Liu,^[a] Chaoqun Bian,^[a] Fang Chen,^[a]
Xiangju Meng,^{*[a]} and Feng-Shou Xiao^{*[a]}

Abstract: Development of sustainable routes for synthesizing aluminophosphate-based zeolites are very important because of their wide applications. As a typical sustainable route, solvent-free synthesis of zeolites not only decreases polluted wastes but also increases product yields. Systematic solvent-free syntheses of hierarchically porous aluminophosphate-based zeolites with AEL and AFI structures is presented. XRD patterns and SEM images show that these samples

have high crystallinity. N₂ sorption isotherm tests show that these samples are hierarchically porous, and their surface areas are comparable with those of corresponding zeolites from hydrothermal route. Chosen as an example, catalytic oxidation of ethylbenzene with O₂ shows that cobalt substituted APO-11 from the solvent-free route (S-CoAPO-11) is more active than conventional CoAPO-11 from hydrothermal route owing to the sample hierarchical porosity.

Introduction

Since the discovery of a new family of microporous crystalline aluminophosphate-based zeolites in the early of 1980s,^[1] they have been paid much attention owing to the variety of structure types and framework composition as well as their applications in catalysis, adsorption, and separation.^[2] As a typical example of this family, APO-11 with AEL-type structure, having one-dimensional 10 membered rings (10MR) of approximately 0.65 × 0.40 nm, has been extensively studied not only because of its advantages such as excellent hydrothermal and thermal stabilities, but also of its easy substitution of tetrahedral framework with a wide range of non-metal and metal ions.^[3] The incorporation of silicon into the framework of APO-11 results in the formation of SAPO-11, which is an industrial catalyst for hydroisomerization of long-chain alkanes owing to the weakly acidic strength and suitable pore size.^[4] The incorporation of metals into the frameworks results in the formation of MAPO-11s, which has been used as effective catalysts for selective oxidations.^[5] APO-5 zeolite with AFI-type structure, having one-dimensional 12 MR channels and its heteroatom-substituted structures, also exhibit good properties in catalysis and adsorption.^[6,7]

Notably, the syntheses of aluminophosphate-based zeolites usually require the presence of solvents such as water and alcohols.^[1–8] The use of these solvents normally produces wastes, reduces synthesis efficiency, and generates high pressure.^[3a] To solve these problems, great efforts have been devoted. For example, Bandyopadhyay et al. reported the synthesis of APO-11 and APO-5 aluminophosphate zeolites from dry gel conversion (DGC),^[8] which could greatly increase the synthesis efficiency, but the process was time-consuming and energy-intensive. Morris et al. developed an ionothermal route for the synthesis of aluminophosphate zeolites such as APO-11, and later, Tian et al. reported the synthesis of APO-5 in the same way.^[9] This route could effectively eliminate the high pressure, but its relatively high cost and slight solubility of silicon limit this method for wide applications.

Recently, Xiao et al. reported a solvent-free synthesis with advantages of reducing the waste production and increasing zeolite yield as well as eliminating high pressure.^[10] More recently, we briefly showed a preliminary work of silicoaluminophosphate SAPO-34 zeolite from the solvent-free route. We reported the details for synthesizing aluminophosphates with AEL and AFI structures and their frameworks substituted with heteroatoms of Si, Co, and Mg under solvent-free conditions.^[11] The samples obtained exhibit comparable properties to those of the samples obtained from conventional hydrothermal route. Particularly, these aluminophosphate-based zeolites synthesized from the solvent-free route are hierarchically porous, which is very favorable for improving catalytic properties.

[a] Y. Jin, X. Chen, Q. Sun, N. Sheng, Dr. Y. Liu, C. Bian, F. Chen, Dr. X. Meng, Prof. F.-S. Xiao
Department of Chemistry, Zhejiang University
Hangzhou 310028 (P. R. China)
E-mail: mengxj@zju.edu.cn
fsxiao@zju.edu.cn

[b] Y. Jin
Department of Analytical Chemistry, Shaoxing University
Shaoxing 312000 (P. R. China)

Supporting information for this article is available on the WWW under
<http://dx.doi.org/10.1002/chem.201403890>.

Results and Discussion

Aluminophosphate zeolite with AEL structure (APO-11)

As a typical example of aluminophosphate zeolites, the solvent-free synthesis of APO-11 was performed by grinding at room temperature and heating at 200 °C for solid compounds of di-*n*-propylamine phosphate (DPA·H₃PO₄) and boehmite. This sample was designated as S-APO-11. Figure 1 shows the sample XRD pattern, N₂ sorption isotherms, SEM and TEM image. The sample XRD pattern exhibits well-resolved peaks in the range of 5–40° (Figure 1A), which is in good agreement with those of the AEL zeolite structure.^[12] After calcined at 600 °C for 4 h, the sample N₂ sorption isotherms exhibit a steep increase in the curve at a relative pressure of 10⁻⁶ < P/P₀ < 0.01, which is due to the filling of micropores.^[3a] Meanwhile, at a relative pressure of 0.45–0.95, a hysteresis loop can be observed, suggesting the presence of mesoporosity and macroporosity in the sample.^[13] Accordingly, BET surface area, pore volume, and BJH pore size distribution are estimated at 212 m²g⁻¹, 0.16 cm³g⁻¹, and about 5 nm, respectively (Table 1).

Table 1. Composition and textural parameters for AEL zeolites synthesized in the absence of solvent.

Samples	Al/P/M (M=Si,Co,Mn) ^[a]	BET surface area [m ² g ⁻¹]	Pore volume [cm ³ g ⁻¹]
S-APO-11	49.9/50.1/—	212	0.16
S-SAPO-11	46.0/45.4/8.6	198	0.18
S-CoAPO-11	43.8/52.6/3.6	175	0.14
S-MnAPO-11	44.9/51.7/3.4	168	0.16

[a] determined by ICP.

SEM microscopy shows that the sample with particle sizes at 1–3 μm aggregated with small particles (200–800 nm, Figure 1C), which could contribute to the formation of macroporosity in the sample. Furthermore, the sample TEM image clearly shows the presence of mesoporosity and macroporosity (Figure 1D). These results are consistent with those in the N₂ sorption isotherm test (Figure 1B).

Figure 2 shows XRD patterns of S-APO-11 samples during the crystallization at 200 °C. Before the crystallization, the sample gives five peaks (7.95°, 13.80°, 21.19°, 24.01°, and 24.22°; Figure 2a) associated with the solid compound of DPA·H₃PO₄. After treatment at 200 °C for 3 h, the peaks of DPA·H₃PO₄ become weak (Figure 2b), at the same time a peak at 6.65° appears, which is related to the interaction between the DPA·H₃PO₄ with Al species. Heating at 200 °C over 6 h, typical peaks assigned to AEL structure appear (Figure 2c,d). With decreasing of the peak at 6.65°, the peaks of AEL structure significantly increase. A further increase in crystallization time to 12 h, the peak at 6.65° completely disappears (Figure 2f). These results suggest that the AEL structure might be transformed from the intermediate at 6.65°. The structure of this intermediate is under investigation. When the crystallization time is over 24 h, there is no obvious change in the XRD pat-

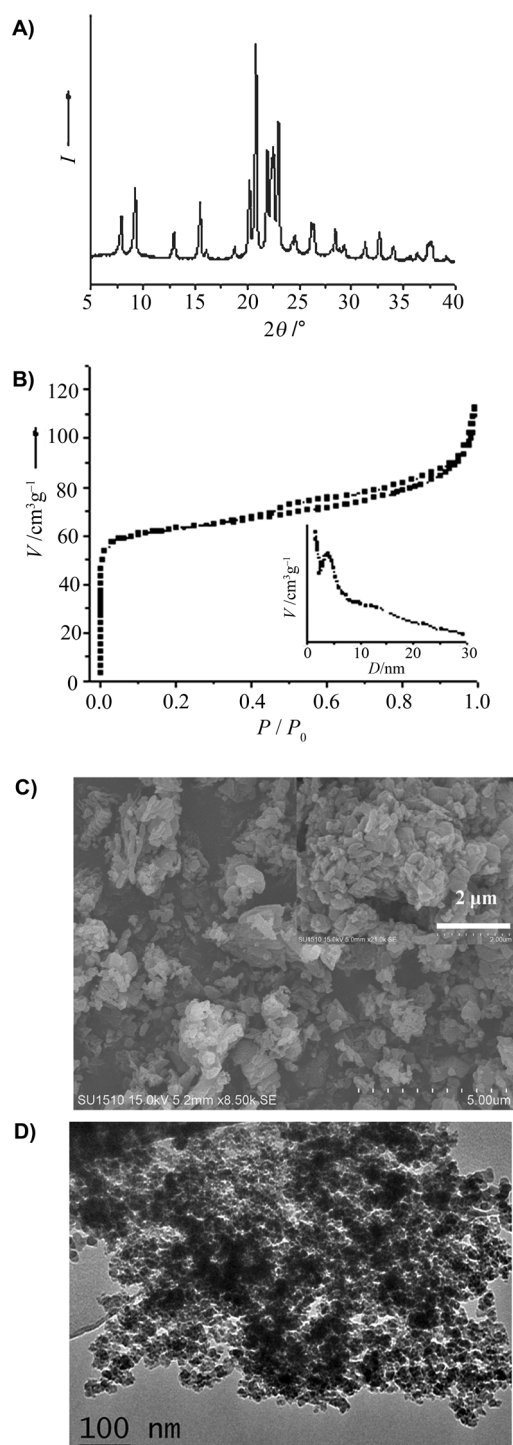


Figure 1. A) XRD pattern, B) N₂ sorption isotherms, C) SEM image, and D) TEM image of an S-APO-11 sample. Inset in (C): Enlargement.

terns (Figure 2 h,i), indicates that the crystallization of S-APO-11 is almost finished at the crystallization time of 24 h.

In the solvent-free synthesis of S-APO-11, the ratio of DPA·H₃PO₄ to Al₂O₃ plays an important role. XRD patterns of S-APO-11 samples crystallized at various ratios of DPA·H₃PO₄ to Al₂O₃ are shown in the Supporting Information, Figure S1. When the ratios are lower than 1.4, there is amorphous phase;

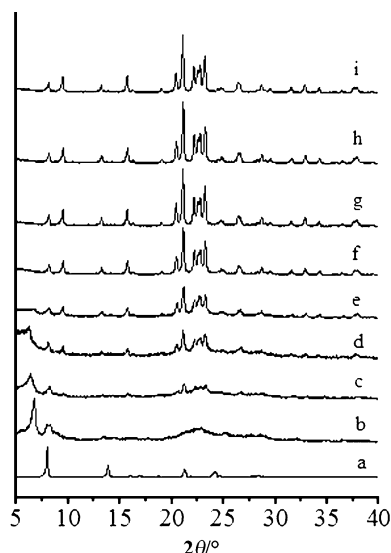


Figure 2. XRD patterns of S-APO-11 samples crystallized at a) 0, b) 3, c) 6, d) 7, e) 9, f) 12, g) 15, h) 24, and i) 36 h.

when the ratios are higher than 1.8, there are impurities such as APO-T; when the ratio reaches to 2.2, it is obtained a pure phase of APO-T. The suitable $\text{DPA}\cdot\text{H}_3\text{PO}_4/\text{Al}_2\text{O}_3$ ratio should be about 1.6. In this case, pure AEL structure with high crystallinity is obtained.

It is worth mentioning that the use of $\text{DPA}\cdot\text{H}_3\text{PO}_4$ is very important for the solvent-free synthesis of aluminophosphate-based zeolites. The $\text{DPA}\cdot\text{H}_3\text{PO}_4$ offers both organic templates and phosphorus source as well as avoidance of amine volatilization in the synthesis.

Heteroatom-substituted APO-11 zeolites

Solvent-free synthesis of silicon-substituted APO-11 was performed by grinding at room temperature and heating at 200°C for 24 h. This sample was designated as S-SAPO-11. Figure 3 shows an XRD pattern, N_2 sorption isotherms, and SEM image of S-SAPO-11 zeolite. The XRD pattern shows that as-synthesized sample has good crystallization with AEL structure. After calcination at 600°C for 4 h, the N_2 sorption isotherms of calcined S-SAPO-11 samples exhibits a steep increase in the curve at a relative pressure of $10^{-6} < P/P_0 < 0.01$ and a hysteresis loop at a relative pressure of 0.85–1.0. The presence of this loop might be related to the macroporosity formed between intercrystals.^[12] The sample BET surface area and pore volume are estimated at $198\text{ m}^2\text{ g}^{-1}$ and $0.18\text{ cm}^3\text{ g}^{-1}$, respectively (Table 1). The sample SEM image shows that the particles are in the range of 1–10 μm , which are formed by aggregation of smaller crystals of 0.1–0.5 μm .

In the solvent-free synthesis of S-SAPO-11, the ratios of both $\text{DPA}\cdot\text{H}_3\text{PO}_4/\text{Al}_2\text{O}_3$ and $\text{SiO}_2/\text{Al}_2\text{O}_3$ strongly influence the sample crystallinity. When $\text{DPA}\cdot\text{H}_3\text{PO}_4/\text{Al}_2\text{O}_3$ ratios are 1.4–1.6 (Supporting Information, Figure S2) and $\text{SiO}_2/\text{Al}_2\text{O}_3$ ratios lower than 0.2 (Supporting Information, Figure S3), the samples give pure AEL structure with high crystallinity.

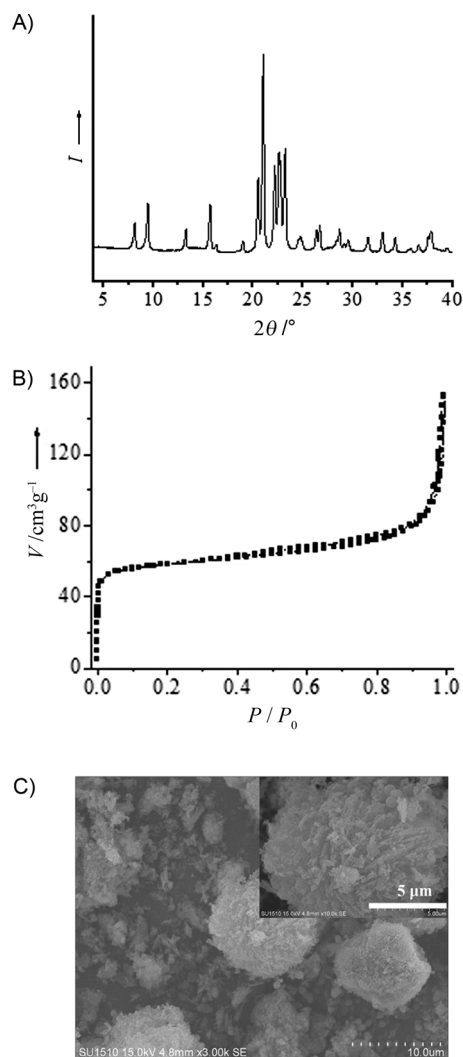


Figure 3. A) XRD pattern, B) N_2 sorption isotherms, and C) SEM image of an S-SAPO-11 sample. Inset: Enlargement.

Figure 4 shows ^{27}Al , ^{31}P , and ^{29}Si MAS NMR spectra of as-synthesized and calcined S-SAPO-11 samples. The ^{27}Al MAS NMR spectrum of as-synthesized S-SAPO-11 (Figure 4A, top) exhibits two peaks at 48.3 and 18.5 ppm. The peak at 48.3 ppm is assigned to four-coordinate Al species in the zeolite framework,^[14] and the peak at 18.5 ppm might be attributed to five-coordinate Al species resulted from the coordination of tetrahedral Al sites with organic templates.^[15] After calcination, the peak at 51.3 ppm is dominant with a shoulder peak at 41.6, both assigned to four-coordinate Al species. The new peak at -5.4 ppm that is due to six-coordinate Al species appears, which is associated with the interaction between the four-coordinate Al species and water molecules (Figure 4A, bottom). This phenomenon is interpreted by that the sample calcination eliminates the coordination of tetrahedral Al species with organic templates, allowing the interaction between the Al species with water to occur. Notably, as-synthesized S-SAPO-11 has much stronger 18.5 ppm peak intensity than conventional SAPO-11 synthesized from hydrothermal route,^[16] suggesting that the interaction of Al species with organic templates in S-

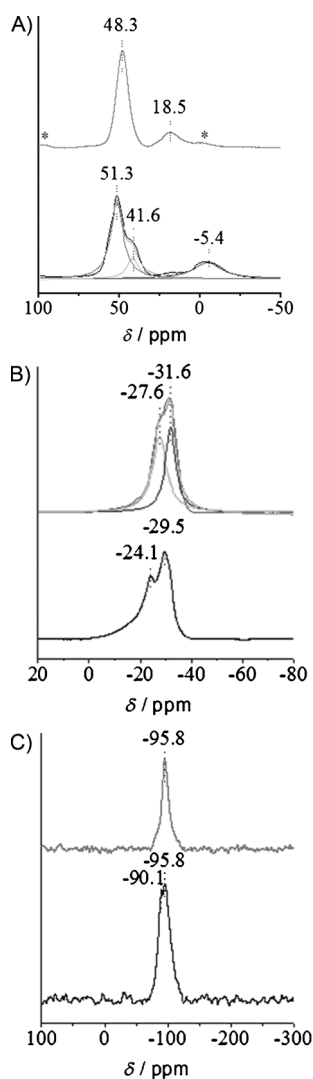


Figure 4. A) ^{27}Al , B) ^{31}P , and C) ^{29}Si NMR spectra of (top) as-synthesized and (bottom) calcined S-SAPO-11 samples (* sideband).

SAPO-11 is much stronger than that in conventional SAPO-11, which may be favorable for filling organic templates in the zeolite framework.

^{31}P NMR spectrum of as-synthesized S-SAPO-11 (Figure 4B, top) exhibits two strong peaks at -31.6 ppm and -27.6 ppm, which are assigned to four-coordinate P species in the zeolite framework.^[17] After calcination, the sample gives peaks at -29.5 ppm and -24.1 ppm. The peaks are obviously shifted to lower, which is explained by the interaction between the four-coordinate P species and water molecules (Figure 4B, bottom).^[17,18]

The ^{29}Si MAS NMR spectrum of as-synthesized S-SAPO-11 (Figure 4C, top) shows a major peak at -95.8 ppm attributed to Si(3Al) species.^[19] After calcination, the calcined sample shows obvious peak at 90.1 ppm associated with Si(4Al) species.^[19] These results suggest that Si species mainly substitute P atoms in the framework of the sample.^[20]

Figure 5A shows XRD patterns of cobalt- and manganese-substituted AEL zeolites from solvent-free synthesis (S-CoAPO-

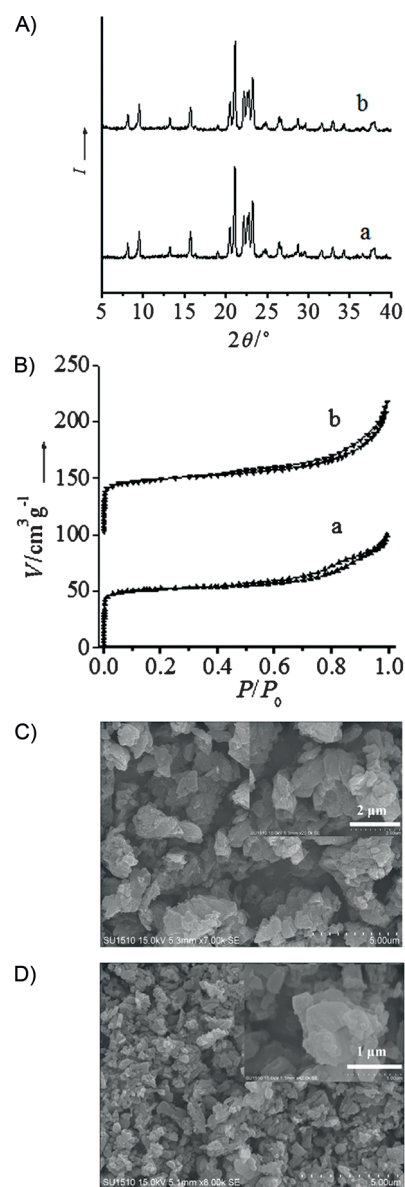


Figure 5. A) XRD patterns, B) N_2 sorption isotherms, C), D) SEM images of a) S-CoAPO-11 and b) S-MnAPO-11 samples (The isotherms for sample b are offset vertically by $100 \text{ cm}^3 \text{ g}^{-1}$). Inset: Enlargement.

11 and S-MnAPO-11). The XRD patterns indicate that these samples have high crystallinity with pure phase. Figure 5B shows N_2 sorption isotherms of calcined S-CoAPO-11 and S-MnAPO-11 samples, and their textural parameters are presented in Table 1. Notably, both S-CoAPO-11 and S-MnAPO-11 samples show a steep increase occurring in the curve at a relative pressure less than 0.01, which is due to the filling of micropores. Furthermore, at a relative pressure of 0.50–0.95, they appear as hysteresis loops, suggesting their hierarchical porosity in the samples (Figure 5B). Their BET surface areas (175 and $168 \text{ m}^2 \text{ g}^{-1}$) are a little lower than that of S-APO-11, which is due to the substitution of the heavy heteroatom in the framework of AEL structure. Figure 5C, D shows SEM images of S-CoAPO-11 and S-MnAPO-11. Both samples are aggregated with smaller crystals (0.5 – $2 \mu\text{m}$ for S-CoAPO-11 and 0.2 – $3 \mu\text{m}$ for S-MnAPO-11).

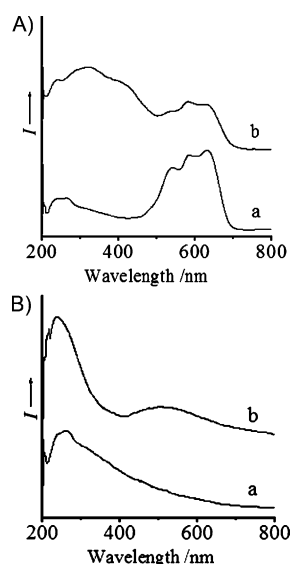


Figure 6. UV/Vis spectra of A) Co- and B) Mn-substituted a) as-synthesized and b) calcined S-MAPO-11 samples (M=Co or Mn).

Figure 6 shows UV/Vis spectra of S-MAPO-11 samples (M=Co and Mn). The absorption bands for as-synthesized S-CoAPO-11 are typical for a perfect tetrahedron $[\text{CoO}_4]$ with one triplet centered at 580 nm (Figure 6A,a), which demonstrates the incorporation of Co^{2+} in the framework.^[21] After calcination, a fraction of the Co species in the framework is oxidized to high-spin tetrahedral Co^{3+} with its characteristic and very intense $\text{O} \rightarrow \text{Co}^{3+}$ charge transfer transitions at around 320 nm and 400 nm (Figure 6A,b).^[21,22] This transformation is also supported by low-temperature ESR spectra (Supporting Information, Figure S4). After oxidation of ethylbenzene with molecular oxygen, the sample has almost no change in the band, indicating a good stability of the cobalt species in the zeolite framework (Supporting Information, Figure S5). As-synthesized S-MnAPO-11 shows a strong band at 260 nm (Figure 6B,a) associated with four-coordinate Mn^{2+} .^[23] After calcination, a new shoulder adsorption at 216 nm appears, which is due to the presence of Mn^{3+} (Figure 6B,b).^[24] These results suggest that both as-synthesized and calcined samples have four-coordinate heteroatoms.

It is well-known that transition metals such as Co species are catalytically active for oxidation of hydrocarbons with molecular oxygen. Table 2 presents catalytic data in a model oxidation of ethylbenzene with molecular oxygen over S-CoAPO-11 and C-CoAPO-11 from the hydrothermal route (Supporting Information, Figure S6), where both samples have similar cobalt contents. The C-CoAPO-11 gives the conversion at 8.3% with product selectivity for acetophenone at 48.6%. In contrast, the S-CoAPO-11 exhibits the conversion at 14.8% with acetophenone selectivity at 77.9%. Obviously, the S-CoAPO-11 is more active and selective than the C-CoAPO-11, which might relate to the unique hierarchical porosity in the S-CoAPO-11. More importantly, there is almost no cobalt leaching in the oxidation (Supporting Information, Table S2). These results indicate that the S-CoAPO-11 has excellent recyclability.

Catalyst ^[a]	Conversion [%]	Selectivity [%]		
		acetophenone	phenyl-ethanol	benzaldehyde
S-CoAPO-11	14.8	77.9	9.7	12.4
C-CoAPO-11	8.3	48.6	16.8	34.6

[a] 2.00 g of ethylbenzene, 0.05 g of catalyst, 0.05 g of *tert*-butyl hydroperoxide solution, 3.0 MPa, 140 °C, 4 h.

Aluminophosphate zeolite with AFI structure (APO-5)

The solvent-free synthesis of APO-5 was performed by grinding at room temperature and heating at 200 °C for solid compounds of di-*n*-propylamine phosphate ($\text{DPA} \cdot \text{H}_3\text{PO}_4$), tetraethylammonium bromide (TEABr), and boehmite. Figure 7 shows an XRD pattern, N_2 sorption isotherms, and SEM image of S-

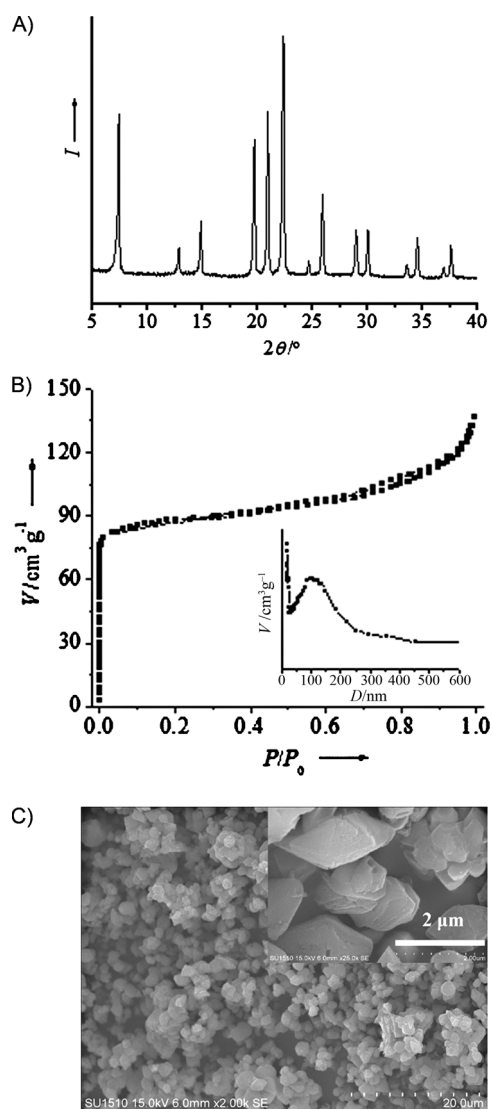


Figure 7. A) XRD pattern, B) N_2 sorption isotherms, and C) SEM image of S-APO-5 sample. Inset: enlargement.

APO-5 zeolite. The sample XRD pattern indicates its good crystallinity with high purity; the sample N_2 sorption isotherms indicate the hierarchical porosity in the S-APO-5; the sample SEM image indicates the aggregative crystals. The BET surface area, pore volume, and BJH pore size distribution are $217 \text{ m}^2 \text{ g}^{-1}$, $0.18 \text{ cm}^3 \text{ g}^{-1}$, and 10 nm, respectively.

It is notable that two templates including both $\text{DPA}\cdot\text{H}_3\text{PO}_4$ and TEABr have been used in the synthesis of S-APO-5. If there is only one template in the synthesis, we cannot obtain the S-APO-5. Clearly, the templation of S-APO-5 require a synergistic effect of $\text{DPA}\cdot\text{H}_3\text{PO}_4$ and TEABr. The details are under investigation.

Heteroatom-substituted APO-5 zeolite

Figure 8 shows XRD pattern, N_2 sorption isotherms, and SEM image of S-SAPO-5. The sample XRD pattern shows strong peaks related to the AFI structure; the sample N_2 sorption isotherms indicate the hierarchical porosity; the sample SEM image gives spherical crystals at 3–5 μm . The sample BET surface area and pore volume are $250 \text{ m}^2 \text{ g}^{-1}$ and $0.17 \text{ cm}^3 \text{ g}^{-1}$.

As presented in the Supporting Information, Table S1, the ratios of $\text{DPA}\cdot\text{H}_3\text{PO}_4/\text{Al}_2\text{O}_3$, $\text{TEABr}/\text{Al}_2\text{O}_3$, and $\text{SiO}_2/\text{Al}_2\text{O}_3$ are strongly dependent on the crystallinity and purity. When the

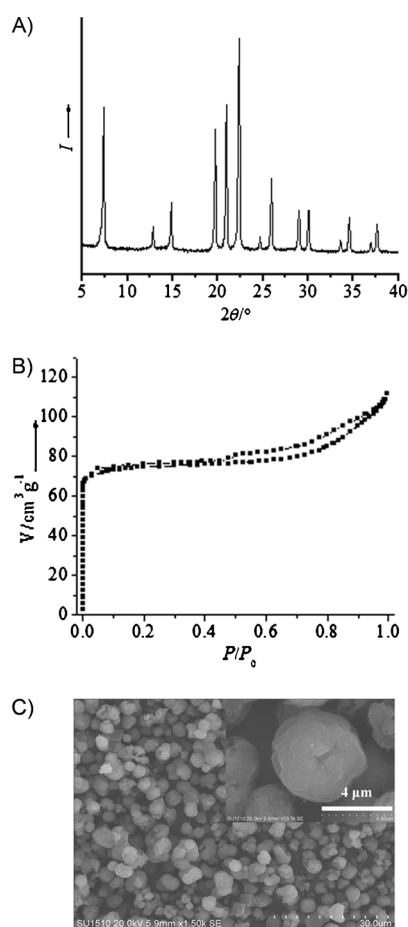


Figure 8. A) XRD pattern, B) N_2 sorption isotherms, and C) SEM image of S-SAPO-5 sample. Inset: enlargement.

ratios of $\text{DPA}\cdot\text{H}_3\text{PO}_4/\text{Al}_2\text{O}_3$ are 1.4–1.8, the ratios of $\text{TEABr}/\text{Al}_2\text{O}_3$ are 0.1–0.4, and the ratios of $\text{SiO}_2/\text{Al}_2\text{O}_3$ are 0.4–1.0, pure S-SAPO-5 with high crystallinity was finally obtained.

Figure 9 shows XRD patterns and SEM images of S-SAPO-5 samples crystallized at various times. After heating at 200°C for 1 h, the sample becomes amorphous because of disappearance of the XRD peaks (Figure 9A,b). Heating at 200°C for 1.5 h results in appearance of a series of weak peaks associated

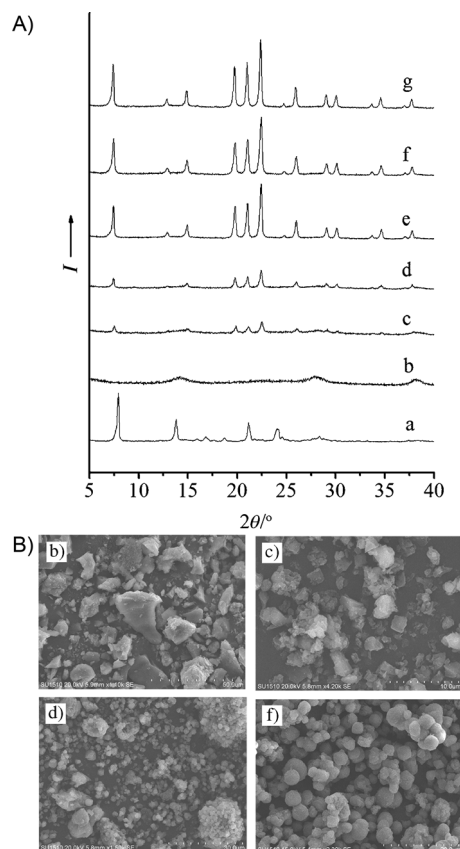


Figure 9. A) XRD patterns and B) SEM images of the samples: a) uncrystallized, b)–g) crystallized at b) 1, c) 1.5, d) 2, e) 3, f) 12, and g) 24 h for synthesizing the S-SAPO-5 sample.

with AFI structure. At the same time, crystals are observed in the sample (Figure 9B,c). These results indicate that a small amount of SAPO-5 crystals have been formed already. Increasing the crystallization time to 3 h, the sample peak intensities increase significantly (Figure 9A,e). A further increase of crystallization time to 12 h, results in disappearance of amorphous phase (Figure 9B,f), indicating full crystallization of the sample (Figure 9A,f). When the crystallization time is over after 12 h, there is no obvious change in the XRD pattern (Figure 9A,g), indicating that the crystallization of S-SAPO-5 is almost finished and that the crystallization of S-SAPO-5 zeolite results from the solid phase transformation.

Figure 10 shows XRD patterns and SEM images of cobalt- and manganese-substituted AFI zeolites (S-CoAPO-5 and S-MnAPO-5). The XRD patterns indicate that they have high crystallinity and purity (Figure 10A), and the SEM images show

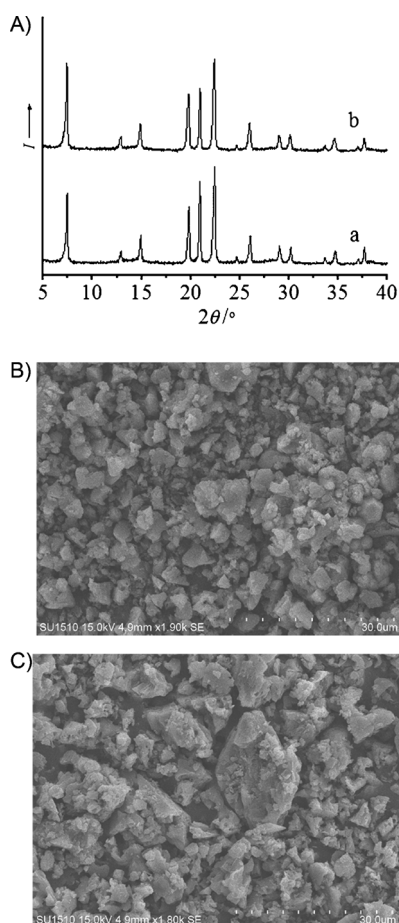


Figure 10. A) XRD patterns, B), C) SEM images of a) S-CoAPO-5 and b) S-MnAPO-5 samples.

their irregular morphology of the crystals (Figure 10B,C). UV/Vis spectra of S-CoAPO-5 and S-MnAPO-5 (Supporting Information, Figure S7) show characteristic peaks related to that the heteroatoms are four-coordinate.

Conclusion

Aluminophosphate zeolites with AEL and AFI structures and their heteroatom-substituted analogues (Si, Co, and Mn) have been successfully synthesized from the solvent-free route through mechanically mixing of solid raw materials, followed by heating in the closed vessel. Compared with the zeolites synthesized from hydrothermal routes, they exhibit similar crystallinity and textural parameters, but their syntheses are simple and product yields are very high. In particular, the solvent-free route results in the formation of hierarchical porosity in the samples, which might be related to relatively fast crystallization and slow diffusion of the solid materials. The formation of the hierarchical porosity is very favorable for mass transfer in catalysis, leading to a significant enhance of catalytic performance. As expected, catalytic tests in oxidation of ethylbenzene with molecular oxygen show that the hierarchically porous S-CoAPO-11 is more active and selective than the conventional CoAPO-11 synthesized from the hydrothermal syn-

thesis. More interestingly, the sample hierarchical porosity is formed in the absence of any mesoscale organic templates. Normally, the formation of the hierarchical porosity in the samples should be created by the mesoscale templates, as reported recently.^[25] The combination of simple process, high yields, and hierarchical porosity in the solvent-free synthesis, would offer a good opportunity for synthesizing various zeolites in the future.

Acknowledgements

We thank the Steady High Magnetic Field Facility (SHMFF), one of the large-scale scientific facilities in Hefei for ESR measurement. This work is supported by the Natural National Science Foundation of China (21422306, 21333009, and 21203165), National High-Tech Research and Development program of China (2013AA065301), Science and Technology Innovative Team of Zhejiang Province (No. 2012R10014-02), and Fundamental Research Funds for the Central Universities (2013XZZX001).

Keywords: AEL structure · aluminophosphate zeolites · APO-11 · heteroatom substitution · solvent-free synthesis

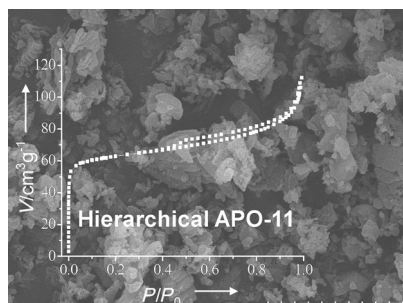
- a) S. T. Wilson, B. M. Lok, C. A. Messina, T. R. Cannan, E. M. Flanigen, *J. Am. Chem. Soc.* **1982**, *104*, 1146–1147; b) S. T. Wilson, B. M. Lok, E. M. Flanigen, *US Patent* **1982**, 4310440; c) W. F. Yan, J. H. Yu, R. R. Xu, G. S. Zhu, F. S. Xiao, Y. Han, K. Sugiyama, O. Terasaki, *Chem. Mater.* **2000**, *12*, 2517–2519; d) J. H. Yu, R. R. Xu, *Acc. Chem. Res.* **2003**, *36*, 481–490.
- a) M. E. Davis, C. Saldarriaga, C. Montes, J. Garces, C. Crowdert, *Nature* **1988**, *331*, 698–699; b) S. J. Miller, *Microporous Mater.* **1994**, *2*, 439–449; c) P. Y. Feng, X. H. Bu, G. D. Stucky, *Nature* **1997**, *388*, 735–741; d) M. Hartmann, L. Kevan, *Chem. Rev.* **1999**, *99*, 635–663; e) N. Wang, Z. K. Tang, G. D. Li, J. S. Chen, *Nature* **2000**, *408*, 426; f) G. Y. Cai, C. L. Sun, Z. M. Liu, C. Q. He, B. L. Luo, Z. Q. Jiang, L. X. Yang, Y. J. Chang, M. L. Gong, R. M. Shi, L. L. Yi, Chinese Patent, **2001**, 96115333.4; g) M. E. Davis, *Nature* **2002**, *417*, 813–821; h) J. H. Yu, R. R. Xu, *Chem. Soc. Rev.* **2006**, *35*, 593–604.
- a) R. R. Xu, W. Q. Pang, J. H. Yu, Q. S. Huo, J. S. Chen, in *Chemistry of Zeolites and Related Porous Materials*, WILEY-VCH, Singapore, **2007**; b) N. J. Tapp, N. B. Milestone, D. M. Bibby, *Zeolites* **1988**, *8*, 183–188; c) M. P. J. Peeters, J. W. de Haan, L. J. M. van de Ven, J. H. C. van Hooff, *J. Phys. Chem.* **1993**, *97*, 5363–5369.
- a) J. M. Campelo, F. Lafont, J. M. Marinas, *Appl. Catal. A* **1998**, *170*, 139–144; b) S. M. Yang, Y. M. Wu, *Appl. Catal. A* **2000**, *192*, 211–220; c) C. M. López, V. Escobar, M. E. Arcos, L. de Nobrega, F. Yáñez, L. V. Garacia, *Catal. Today* **2008**, *133–135*, 120–128.
- a) C. A. Messina, B. M. Lok, E. M. Flanigen, US Patent, **1985**, 4554143; b) S. T. Wilson, E. M. Flanigen, US Patent, **1986**, 4567029; c) P. T. Barger, S. T. Wilson, J. S. Holmgren, US Patent, **1992**, 5126308; d) M. da S. Machado, J. Pérez-Pariante, E. Sastre, D. Cardoso, M. V. Giotto, J. L. García-Fierro, V. Fornés, *J. Catal.* **2002**, *205*, 299–308; e) P. Tian, Z. M. Liu, Z. B. Wu, L. Xu, Y. L. He, *Catal. Today* **2004**, *93–95*, 735–742; f) W. B. Fan, R. F. Li, T. Dou, T. Tatsumi, B. M. Weckhuysen, *Microporous Mesoporous Mater.* **2005**, *84*, 116–126.
- a) S. L. Qiu, W. Q. Pang, H. Kessler, J. L. Guth, *Zeolites* **1989**, *9*, 440–444; b) G. Finger, J. Richter-Mendau, M. Bülow, J. Kornatowski, *Zeolites* **1991**, *11*, 443–448; c) I. Girnus, M. M. Pohl, J. Richter-Mendau, M. Schneider, M. Noack, D. Venzke, J. Caro, *Adv. Mater.* **1995**, *7*, 711–714; d) I. Girnus, K. Jancke, R. Vetter, J. Richter-Mendau, J. Caro, *Zeolites* **1995**, *15*, 33–39; e) H. Li, G. S. Zhu, X. D. Guo, Y. Li, C. J. Li, S. L. Qiu, *Microporous Mesoporous Mater.* **2005**, *85*, 324–330.
- a) T. C. Xiao, L. D. An, H. L. Wang, *Appl. Catal. A* **1995**, *130*, 187–194; b) M. Höchtl, A. Jentys, H. Vinek, *Appl. Catal. A* **2001**, *207*, 397–405; c) W. B. Fan, R. F. Li, T. Dou, T. Tatsumi, B. M. Weckhuysen, *Microporous*

- Mesoporous Mater.* **2005**, *84*, 116–126; d) L. J. Wang, C. W. Guo, S. R. Yan, X. D. Huang, Q. Z. Li, *Microporous Mesoporous Mater.* **2003**, *64*, 63–68; e) Q. Yang, M. Li, C. F. Zeng, L. X. Zhang, *Chem. Eur. J.* **2012**, *18*, 365–371.
- [8] a) M. Bandyopadhyay, R. Bandyopadhyay, Y. Kubota, Y. Sugi, *Chem. Lett.* **2000**, *29*, 1024–1025; b) R. Bandyopadhyay, M. Bandyopadhyay, Y. Kubota, Y. Sugi, *J. Porous Mater.* **2002**, *9*, 83–95.
- [9] a) E. R. Cooper, C. D. Andrews, P. S. Wheatley, P. B. Webb, P. Wormald, R. E. Morris, *Nature* **2004**, *430*, 1012–1016; b) L. Wang, Y. P. Xu, Y. Wei, J. C. Duan, A. B. Chen, B. C. Wang, H. J. Ma, Z. J. Tian, L. W. Lin, *J. Am. Chem. Soc.* **2006**, *128*, 7432–7433.
- [10] L. M. Ren, Q. M. Wu, C. G. Yang, L. F. Zhu, C. J. Li, P. L. Zhang, H. Y. Zhang, X. Q. Meng, F. S. Xiao, *J. Am. Chem. Soc.* **2012**, *134*, 15173–15176.
- [11] Y. Y. Jin, Q. Sun, G. D. Qi, C. G. Yang, J. Xu, F. Chen, X. Q. Meng, F. Deng, F. S. Xiao, *Angew. Chem. Int. Ed.* **2013**, *52*, 9172–9175; *Angew. Chem.* **2013**, *125*, 9342–9345.
- [12] C. Baerlocher, L. B. McCusker, D. H. Olson, in *Atlas of Zeolite Framework Types*, 6th rev. ed., ELSEVIER, Amsterdam, **2007**.
- [13] O. Sel, D. Kuang, M. Thommes, B. Smarsly, *Langmuir* **2006**, *22*, 2311–2322.
- [14] a) A. M. Prakash, S. Unnikrishnan, *J. Chem. Soc. Faraday Trans.* **1994**, *90*, 2291–2296; b) A. Buchholz, W. Wang, M. Xu, A. Arnold, M. Hunger, *Microporous Mesoporous Mater.* **2002**, *56*, 267–278; c) G. Liu, P. Tian, Y. Zhang, J. Li, L. Xu, S. Meng, Z. Liu, *Microporous Mesoporous Mater.* **2008**, *114*, 416–423.
- [15] a) C. S. Blackwell, R. L. Patton, *J. Phys. Chem.* **1984**, *88*, 6135–6139; b) C. S. Blackwell, R. L. Patton, *J. Phys. Chem.* **1988**, *92*, 3965–3970.
- [16] A. K. Sinha, S. Seelan, *Appl. Catal. A* **2004**, *270*, 245–252.
- [17] a) D. Hasha, L. S. de Saldarriaga, C. Saldarriaga, P. E. Hathaway, D. F. Cox, M. E. Davis, *J. Am. Chem. Soc.* **1988**, *110*, 2127–2135; b) Y. Huang, D. Machado, C. W. Kirby, *J. Phys. Chem. B* **2004**, *108*, 1855–1865.
- [18] a) H. L. Zubowa, E. Alsdorf, R. Fricke, F. Neissendorfer, J. Richter-Mendau, E. Schreier, D. Zeigan, B. Zibrowius, *J. Chem. Soc. Faraday Trans.* **1990**, *86*, 2307–2312; b) Y. Watanabe, A. Koiwai, H. Takeuchi, S. A. Hyodo, S. Noda, *J. Catal.* **1993**, *143*, 430–436.
- [19] a) R. B. Borade, A. Clearfield, *J. Mol. Catal.* **1994**, *88*, 249–265; b) J. Tan, Z. Liu, X. Bao, X. Liu, X. Han, C. He, R. Zhai, *Microporous Mesoporous Mater.* **2002**, *53*, 97–108.
- [20] M. Briend, R. Vomscheid, M. J. Peltre, P. P. Man, D. Barthomeuf, *J. Phys. Chem.* **1995**, *99*, 8270–8276.
- [21] a) M. G. Uytterhoeven, R. A. Schoonheydt, *Microporous Mater.* **1994**, *3*, 265–279; b) A. A. Verberckmoes, B. M. Weckhuysen, R. A. Schoonheydt, *Microporous Mesoporous Mater.* **1998**, *22*, 165–178; c) B. M. Weckhuysen, R. R. Rao, J. A. Martens, R. A. Schoonheydt, *Eur. J. Inorg. Chem.* **1999**, 565–577; d) W. B. Fan, R. A. Schoonheydt, B. M. Weckhuysen, *Phys. Chem. Phys.* **2001**, *3*, 3240–3246; e) D. Grandjean, A. M. Beale, A. V. Petukhov, B. M. Weckhuysen, *J. Am. Chem. Soc.* **2005**, *127*, 14454–14465.
- [22] a) A. M. Prakash, S. V. V. Chilukuri, S. Ashtekar, D. K. Chakrabarty, *J. Chem. Soc. Faraday Trans.* **1996**, *92*, 1257–1262; b) C. Montes, M. E. Davis, B. Murray, M. Narayana, *J. Phys. Chem.* **1990**, *94*, 6431–6435.
- [23] N. Rajič, D. Stojaković, S. Hocevar, V. Kaučič, *Zeolites* **1993**, *13*, 384–387.
- [24] B. Modén, L. Oliviero, J. Dakka, J. G. Santiesteban, E. Iglesia, *J. Phys. Chem. B* **2004**, *108*, 5552–5563.
- [25] a) Y. Tao, H. Kanoh, L. Abrams, K. Kaneko, *Chem. Rev.* **2006**, *106*, 896–910; b) J. Pérez-Ramírez, C. H. Christensen, K. Egeblad, C. H. Christensen, J. C. Groen, *Chem. Soc. Rev.* **2008**, *37*, 2530–2542; c) K. Möller, T. Bein, *Chem. Soc. Rev.* **2013**, *42*, 3689–3707.

Received: June 10, 2014
Revised: August 13, 2014
Published online on ■ ■ ■, 0000

FULL PAPER

Hierachically porous aluminophosphate-based zeolites with AEL and AFI structures have been successfully synthesized by a solvent-free route. Catalysis tests in the oxidation of ethylbenzene with molecular oxygen show that S-CoAPO-11 is more active than conventional CoAPO-11 from the hydrothermal route.



Zeolite Synthesis

Y. Jin, X. Chen, Q. Sun, N. Sheng, Y. Liu, C. Bian, F. Chen, X. Meng,* F.-S. Xiao*



Solvent-Free Syntheses of Hierarchically Porous Aluminophosphate-Based Zeolites with AEL and AFI Structures

